Electron-phonon interaction in disordered conductors: Static and vibrating scattering potentials

A. Sergeev and V. Mitin
Department of ECE, Wayne State University, Detroit, Michigan 48202
(Received 2 July 1999; revised manuscript received 23 September 1999)

Employing the Keldysh diagram technique, we calculate the electron-phonon energy relaxation rate in a conductor with the vibrating and static δ-correlated random electron-scattering potentials. If the scattering potential is completely dragged by phonons, this model yields the Schmid's result for the inelastic electron-scattering rate $\tau_{e\text{-}ph}^{-1}$. At low temperatures the effective interaction decreases due to disorder, and $\tau_{e\text{-}ph}^{-1} \propto T^4 l$ (l is the electron mean-free path). In the presense of the static potential, quantum interference of numerous scattering processes drastically changes the effective electron-phonon interaction. In particular, at low temperatures the interaction increases, and $\tau_{e\text{-}ph}^{-1} \propto T^2/l$. Along with an enhancement of the interaction, which is observed in disordered metallic films and semiconducting structures at low temperatures, the suggested model allows us to explain the strong sensitivity of the electron relaxation rate to the microscopic quality of a particular film.

I. INTRODUCTION

Electron-phonon scattering plays a key role in the description of many phenomena, such as electron dephasing, heat removal from hot electrons, superconducting branch imbalance relaxation, etc. Although well characterized in clean bulk conductors, the current understanding in disordered and nanoscale systems is limited.

Electron scattering from impurities and boundaries destroys the single-particle picture of electron-phonon interaction. Along with the process of ''pure'' electron-phonon scattering, which takes place in pure conductors, there is the other basic process, namely, the inelastic electron scattering from vibrating impurities, defects, and boundaries. Together with elastic electron scattering and pure electron-phonon scattering, this mechanism generates a wide variety of interference processes. If the electron-scattering potential (impurities, defects, and boundaries) is completely dragged by phonons, the inelastic electron-impurity scattering may be excluded by a unitary transformation to a frame of reference, which moves with the phonon mode under consideration. Exploiting this transformation, Schmid[1] has found that in the presence of strong disorder ($q_T l < 1, q_T$ is the wave vector of a thermal phonon) the electron-phonon interaction becomes weaker, and the energy relaxation rate $\tau_{e\text{-}ph}^{-1}$ is of the order of $(q_T l)\tau_0^{-1} \propto T^4 l$ ($\tau_0^{-1} \propto T^3$ is the relaxation rate in pure material). As emphasized in Refs. 2–4, this conclusion is consistent with the Pippard's famous result for the ultrasonic attenuation coefficient. It was also demonstrated[2,5] that the correct calculations lead to Schmid's result and the Pippard formula independent of the reference frame used.

Detailed studies show that many experimental results may be understood in the frame of the available theory.[6–8] However, a set of low-temperature observations is in strong disagreement with current theoretical understanding of the electron-phonon interaction in disordered conductors. Enhancement of the interaction due to disorder has been found in two-dimensional electron gas (2DEG) in GaAs/Al-Ga-As heterojunctions with $l = 0.3 - 0.8$ μm below 0.5 K,[9] and in bulk $Ti_{1-x}Al_x$ alloys with values of l ranged from 0.26 to 1.1 nm at $T = 3$–10 K.[10] The T^2 dependence of the relaxation rate is widely observed in experiments. In some cases it may be associated with the contribution of transverse phonons in the pure limit $q_T l > 1$, predicted by the theory. Recent measurements[11] show that this dependence takes place even in the deep impure limit $q_T l \sim 0.01$, where T^4 dependence is expected.

As the current theory is self-consistent, the search for reasons behind this discrepancy should turn to the model assumptions. Many-body corrections to phonon states were considered in Ref. 12. It has been found that the modification of the electron relaxation rate occurs only under a strong phonon damping. On the electronic side, the main model assumption of the current theory is that the scattering potential is completely dragged by phonons. This assumption may be wrong for structures with heavy defects and tough boundaries. That is why one can expect the relaxation rate to be modified in nonhomogeneous conductors and nanoscale structures.

To study the effects of incomplete drag of scatterers by phonons we consider the model taking into account the vibrating and static δ-correlated random-scattering potentials. One of the effects originating from elastic electron scattering is well understood now. The diffusion motion of electrons makes the interaction time longer, which enhances an interaction. Renormalization of the ''pure'' electron-phonon vertex due to electron-impurity scattering has been calculated in Ref. 13. Here we study all electron-phonon interference processes, with taking into account the renormalization of all vertices as well as the modification of electron screening due to disorder.

The outline of this paper is as follows. Starting with bare vertices of electron scattering from phonons, the static and vibrating potentials, we consider screening of these vertices and build effective vertices of the electron-phonon interaction in Sec. II. The energy relaxation rate in a disordered conductor is calculated in Sec. III. Discussion of our main results and comparison with experiment are presented in Sec. IV.

II. MODEL HAMILTONIAN AND EFFECTIVE VERTICES

We consider electron scattering from the static and vibrating potentials, assuming that the vibrating potential is completely dragged by thermal phonons. To keep terminology of previous papers and distinguish between these potentials, we attribute the vibrating potential to ''impurities.'' Keeping in mind that the vibrating potential has static and dynamic components, we associate elastic electron-impurity scattering and inelastic electron-impurity scattering with the static and dynamic components correspondently. Thus, the electron momentum relaxation rate (elastic relaxation rate) is determined by the static potential and the static component of electron-impurity potential. Inelastic electron-impurity scattering (scattering of electrons from vibrating impurities) induces a new channel of the electron-phonon interaction. Screening of the bare electron-phonon interaction as well as some interaction processes generated by the inelastic electron-impurity scattering is strongly dependent on the elastic relaxation rate. Because of a significant effect of elastic electron scattering on the dielectric function, we should start our consideration with bare (unscreened) vertices.

Following Refs. 2 and 5, we study the Hamiltonian, which includes electron-electron ($V^o_{e\text{-}e}$) and bare electron-phonon (B°) scattering, elastic ($V^o_{e\text{-}imp}$) and inelastic (γ°) electron scattering from impurities dragged by phonons. With additional static potential (V_{st}), this Hamiltonian has a form

$$
\begin{aligned}
H_{int}=&(1/2)\sum_{\mathbf{p},\mathbf{p}',\mathbf{k}} V^o_{e\text{-}e}(\mathbf{k})c^\dagger_{\mathbf{p}}c^\dagger_{\mathbf{p}'}c_{\mathbf{p}'+\mathbf{k}}c_{\mathbf{p}-\mathbf{k}}\\
&+\sum_{\mathbf{p},\mathbf{q}} B^o(\mathbf{q})c^\dagger_{\mathbf{p}+\mathbf{q}}c_{\mathbf{p}}(b_{\mathbf{q},n}+b^\dagger_{-\mathbf{q},n})+\sum_{\mathbf{p},\mathbf{k}} V_{st}(\mathbf{k})c^\dagger_{\mathbf{p}}c_{\mathbf{p}-\mathbf{k}}\\
&+\sum_{\mathbf{p},\mathbf{k},\mathbf{R}_\alpha} V^o_{e\text{-}imp}(\mathbf{k})c^\dagger_{\mathbf{p}}c_{\mathbf{p}-\mathbf{k}}\exp(-i\mathbf{k}\mathbf{R}_\alpha)\\
&+\sum_{\mathbf{p},\mathbf{k},\mathbf{q},\mathbf{R}_\alpha} \gamma^o(\mathbf{k},\mathbf{q})c^\dagger_{\mathbf{p}}c_{\mathbf{p}-\mathbf{k}}(b_{\mathbf{q},n}+b^\dagger_{-\mathbf{q},n})\\
&\times\exp[-i(\mathbf{k}-\mathbf{q})\mathbf{R}_\alpha],
\end{aligned}
\tag{1}
$$

where $c^\dagger_{\mathbf{p}}$ is the electron creation operator, $b^\dagger_{\mathbf{q},n}$ is the creation operator of a phonon with a wave vector $\mathbf{q}$ and polarization index n, and $\mathbf{R}_\alpha$ are the equilibrium positions of impurities, which are dragged by phonons.

The unscreened vertices of electron-electron, electron-impurity, and electron-phonon scattering are given by

$$
V^o_{e\text{-}e}(\mathbf{k})=\frac{4\pi e^2}{k^2},\quad V^o_{e\text{-}imp}(k)=-\frac{4\pi e^2(Z_{imp}-Z_{ion})}{k^2},
\tag{2}
$$

$$
B^o(\mathbf{q})=-\frac{iV^o_{e\text{-}ion}(q)N\mathbf{q}\mathbf{e}_n}{(2\rho\omega_q)^{1/2}},\quad V^o_{e\text{-}ion}(\mathbf{q})=-\frac{4\pi Z_{ion}}{q^2},
\tag{3}
$$

where $V^o_{e\text{-}im}$ is the bare electron-impurity scattering potential, $\mathbf{e}_n$ is the phonon polarization vector, N is the number of unit cells, ρ is the density.

The bare vertex of inelastic electron-impurity scattering is given by[2,5]

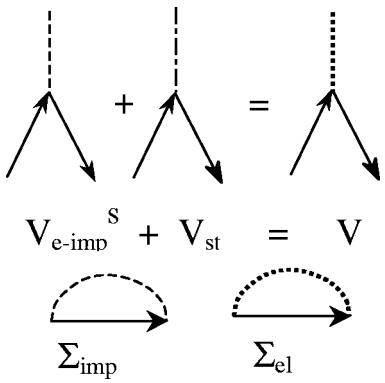

FIG. 1. Electron vertices and self-energies describing elastic electron scattering from impurities and the static potential.

$$
\gamma^o(\mathbf{k},\mathbf{q})=-iV^o_{e\text{-}imp}(\mathbf{k}\mathbf{e}_n)/(2\rho\omega_q)^{1/2}.
\tag{4}
$$

The vertices of elastic and inelastic electron-impurity scattering describe processes with large electron momentum transferred to impurities ($k\sim p_F$). In the case $kl\gg 1$, the dielectric function corresponds to the static limit,

$$
\epsilon(k)=1+\kappa^2/k^2,\quad \kappa^2=4\pi e^2\nu,\quad \nu=mp_F/\pi^2.
\tag{5}
$$

Therefore, the screened impurity potential is given by

$$
V^s_{e\text{-}imp}=-4\pi(Z_{imp}-Z_{ion})/\kappa^2.
\tag{6}
$$

The screened vertex of inelastic electron-impurity scattering is obtained from Eq. (4) by substituting $V^o_{e\text{-}imp}$ by $V^s_{e\text{-}imp}$. Assuming that the static potential is already screened, we add it to the screened impurity potential, as it is shown in Fig. 1. Then the electron momentum relaxation rate is determined by the total potential: $V=V_{st}+V^s_{e\text{-}imp}$.

To build effective vertices and consider the electron-phonon relaxation we employ the Keldysh diagrammatic technique.[14] In the Keldysh technique for nonequilibrium processes the electron and phonon Green functions (G and D), the electron self-energy (Σ) and the polarization operator (P) are represented by matrices

$$
\hat{G}=\begin{pmatrix} 0 & G^A \\ G^R & G^C \end{pmatrix},\quad \hat{D}=\begin{pmatrix} 0 & D^A \\ D^R & D^C \end{pmatrix},
\tag{7}
$$

$$
\hat{\Sigma}=\begin{pmatrix} \Sigma^C & \Sigma^R \\ \Sigma^A & 0 \end{pmatrix},\quad \hat{P}=\begin{pmatrix} P^C & P^R \\ P^A & 0 \end{pmatrix},
\tag{8}
$$

where A and R stand for advanced and retarded components of the matrix function and C corresponds to the kinetic component.

The retarded (advanced) component of the electron Green function taking into account the elastic electron scattering is given by

$$
G^R_0(\mathbf{p},\epsilon)=[G^A_0(\mathbf{p},\epsilon)]^*=(\epsilon-\xi_p+i/2\tau)^{-1},
\tag{9}
$$

where $\xi_p=(p^2-p_F^2)/2m$. The total momentum relaxation rate, $1/\tau$, is determined by electron scattering from impurities and also from the static potential. In the diagrammatic presentation shown in Fig. 1, the momentum relaxation rate is given by the imaginary part of the electron self-energy dia-

gram Σ_{el}, which includes both the static impurity potential, $V^s_{e\text{-}imp}$, and additional static potential, V_{st}. Thus, we have

$$1/\tau = 2\ \mathrm{Im}\Sigma^A_{el},\quad l = v_F\tau. \tag{10}$$

It is convenient to describe the potential of vibrating impurities by the corresponding electron momentum relaxation rate,

$$\tilde{\tau}^{-1} = \pi\nu N_{im}(V^s_{e\text{-}im})^2,\quad \tilde{l} = v_F\tilde{\tau}, \tag{11}$$

where N_{im} is the concentration of impurities dragged by thermal phonons. In other words, the electron momentum relaxation rate with respect to scattering from impurities is given by the electron self-energy Σ_{imp}, shown on Fig. 1. As we will see, the parameter

$$k = \tau/\tilde{\tau} = l/\tilde{l} \tag{12}$$

plays a key role in modification of the electron-phonon interaction.

The retarded component of the phonon Green functions is

$$D^R(\mathbf{q},\omega) = (\omega - \omega_{\mathbf{q}} + i0)^{-1} + (\omega + \omega_{\mathbf{q}} + i0)^{-1}. \tag{13}$$

Studying the electron energy relaxation in an impure conductor, we focus our attention on the time scale, which is much longer than the electron momentum relaxation time τ. Then the kinetic Green function may be presented as

$$G^C(\mathbf{p},\epsilon) = (2n_\epsilon + 1)2i\ \ \mathrm{Im}G^A(\mathbf{p},\epsilon), \tag{14}$$

where n_ϵ is the isotropic electron distribution function.

We assume that the phonon subsystem is in equilibrium. It is realized at temperatures $T \geqslant 10$ K due to large heat capacity of phonons, or in thin films, if the phonon escape time is shorter than the phonon-electron relaxation time. In equilibrium,

$$D^C(\mathbf{q},\omega) = (2N_\omega + 1)2i\ \mathrm{Im}D^R(\mathbf{q},\omega), \tag{15}$$

where $N_\omega = [\exp(\omega/T) - 1]^{-1}$ is the phonon equilibrium distribution function.

In the Keldysh technique all bare vertices, as well as the screened vertix $\gamma(\mathbf{k},\mathbf{q})$ are multiplied by the tensor

$$K^1_{ij} = \delta_{ij}/\sqrt{2},\quad K^2_{ij} = (\sigma_x)_{ij}/\sqrt{2}, \tag{16}$$

with an upper phonon index and lower electron indices. In what follows, we will present only vertex components with phonon index $k = 2$. In the canonical collision integral, these components give a term, which is proportional to $(2N_\omega + 1)(n_{\epsilon+\omega} - n_\epsilon)$.

Now we consider screening of the electron-phonon vertex $B(\mathbf{q},\omega)$ with a small value of the transferred momentum, $q \sim T/u$. Screening of the electron-electron potential in the frame of random phase approximation is presented in Fig. 2; the corresponding equation has a form

$$V^R(\mathbf{q},\omega) = [V^A(\mathbf{q},\omega)]^* = V^o_{e\text{-}e}(\mathbf{q})/\epsilon^R(\mathbf{q},\omega), \tag{17}$$

$$\epsilon^R(q,\omega) = 1 - V^o_{e\text{-}e}(q)P^A_0(q,\omega), \tag{18}$$

where the electron polarization operator shown in Fig. 2 is given by

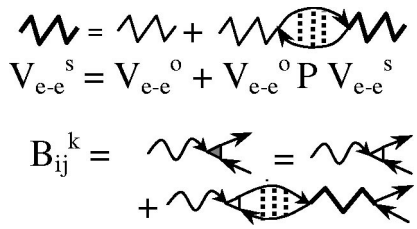

FIG. 2. Screening of the electron-electron potential ($V^o_{e\text{-}e}$) and vertex of bare electron-phonon interaction (B°).

$$P^A_0(q,\omega) = -\nu\frac{1 - \zeta^*_0(q,\omega) - i\omega\tau\zeta^*_0(q,\omega)}{1 - \zeta^*_0(q,\omega)}. \tag{19}$$

Here we introduce the following notations for integrals of electrons Green functions

$$\zeta_n = \frac{1}{\pi\nu\tau}\int\frac{d\mathbf{p}}{(2\pi)^3}G^A(\mathbf{p},\epsilon)G^R(\mathbf{p}+\mathbf{q},\epsilon+\omega)y^n, \tag{20}$$

where $y = (\mathbf{p}\cdot\mathbf{q})/(pq)$. Note, that

$$\zeta_1 = (1 - \zeta_0 + i\omega\tau\zeta_0)/(iql), \tag{21}$$

$$\zeta_2 = \frac{1 - i\omega\tau}{(ql)^2}(1 - \zeta_0 + i\omega\tau\zeta_0). \tag{22}$$

Screening of the vertex of bare electron-phonon interaction is shown in Fig. 2. Using Eqs. (3), (18), and (29), we obtain the screened vertex $B(\mathbf{q},\omega)$,

$$B^2_{ij} = \frac{(B^o)^2_{ij}}{\epsilon^A(\mathbf{q},\omega)} = \frac{ig}{\sqrt{2}}\frac{1 - \zeta^*_0}{1 - \zeta^*_0 - i\omega\tau\zeta^*_0}, \tag{23}$$

where the constant g coincides with coupling constant in pure metals:

$$g = \frac{2\epsilon_F}{3}\frac{\mathbf{q}\cdot\mathbf{e}_n}{(2\rho\omega)^{1/2}} \tag{24}$$

Now, following Ref. 2, we build effective vertices shown in Fig. 3. The vertex Γ, taking into account elastic and inelastic electron-impurity scattering, is

$$\Gamma^2_{11} = \frac{\mathbf{p}\cdot\mathbf{e}_n}{\tilde{\tau}(\rho\omega)^{1/2}}(n_\epsilon - n_{\epsilon+\omega}), \tag{25}$$

for $k = 2$; all other components are zero.

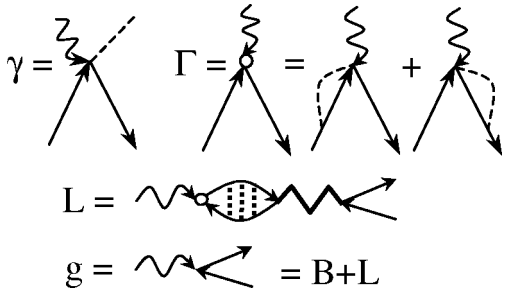

FIG. 3. Effective vertices of the electron-phonon interaction γ, Γ, L, and g.

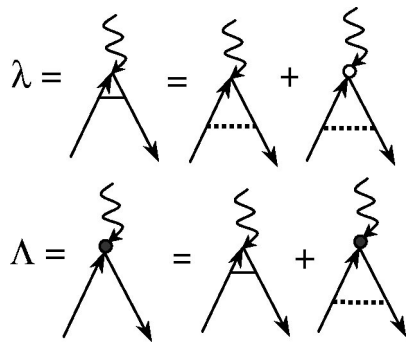

FIG. 4. Vertex Λ, obtained after renormalization of vertices Γ and g due to elastic electron scattering.

Using the vertex Γ^k_{ij}, one can build the vertex L^k_{ij}. As it is seen from Fig. 2, the vertex L^k_{ij} in the limit of strong screening is given by

$$L^2_{ij}=-\frac{i\omega P_F(\tau/\tilde{\tau})\zeta_1^*}{1-(1-i\omega\tau)\zeta_0^*}\frac{\delta_{ij}}{2(\rho\omega)^{1/2}}=\frac{g}{\sqrt{2}}\frac{3\omega\tau}{ql}\frac{\tau}{\tilde{\tau}}\delta_{ij}. \tag{26}$$

The vertices B^k_{ij} and L^k_{ij} have the same index structure in the Keldysh space. Summing up these vertices, we get the vertex g^k_{ij} with components

$$g^2_{ij}=\frac{ig}{\sqrt{2}}\left[1+i\omega\tau\left(\frac{\zeta_0^*}{1-\zeta_0^*-i\omega\tau\zeta_0^*}-\frac{3}{(ql)^2}\frac{\tau}{\tilde{\tau}}\right)\right]\delta_{ij}. \tag{27}$$

The vertices Γ^k_{ij} and g^k_{ij} are strongly renormalized due to elastic electron scattering. To calculate the renormalized vertex, one needs to introduce the vertex λ^k_{ij} with the one electron-impurity scattering and to solve an equation shown in Fig. 4 for the vertex Λ^k_{ij} (the vertex Γ^k_{ij} has a vector character; it cannot be renormalized directly). Using Eqs. (25) and (27), we find

$$\lambda^2_{11}=\frac{2ig}{\sqrt{2}}\left(\frac{\zeta_0^*}{1-\zeta_0^*-i\omega\tau\zeta_0^*}-\frac{3}{(ql)^2}\frac{\tau}{\tilde{\tau}}\right)(1-\zeta_0^*)(n_\epsilon-n_{\epsilon+\omega}), \tag{28}$$

$$\Lambda^2_{11}=\frac{2ig}{\sqrt{2}}\left(\frac{\zeta_0^*}{1-\zeta_0^*-i\omega\tau\zeta_0^*}-\frac{3}{(ql)^2}\frac{\tau}{\tilde{\tau}}\right)(n_\epsilon-n_{\epsilon+\omega}). \tag{29}$$

Thus, we have found effective vertices γ,Γ,g,Λ, which will be used in the next section to calculate the electron-phonon relaxation rate.

III. ELECTRON ENERGY RELAXATION

The kinetic equation for the electron distribution function n_ϵ has a form[13]

$$\frac{dn_\epsilon}{dt}=\frac{i}{\pi\nu}\int\frac{d\mathbf{p}}{(2\pi)^3}\mathrm{Im}G^A(\mathbf{p},\epsilon)[2i(2n_\epsilon-1)\mathrm{Im}\Sigma^A(\mathbf{p},\epsilon)-\Sigma^C(\mathbf{p},\epsilon)], \tag{30}$$

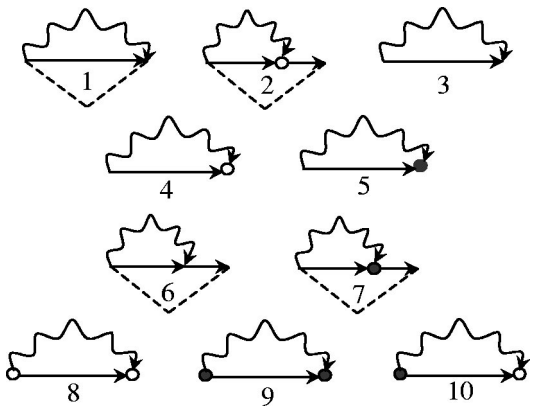

FIG. 5. Electron self-energy diagrams.

where the right-hand side of the last equation is the collision integral $I(\epsilon)$ expressed through the electron self-energy [$\Sigma^{A(C)}$ is the advanced (kinetic) electron-phonon self-energy]. All possible electron-phonon self-energy diagrams with vertices γ,Γ,g,Λ are presented in Fig. 5.

Let us first consider the interaction of electrons and transverse phonons. Only the first and second diagrams with vertices γ and Γ give contributions to this interaction. The collision integral based on the first self-energy diagram with two vertices $\gamma(\mathbf{k},\mathbf{q})$ is

$$I_1(\epsilon)=\frac{8}{\pi\nu}\int\frac{d\mathbf{p}d\mathbf{k}d\mathbf{q}d\omega}{(2\pi)^9}[\gamma(\mathbf{k},q)]^2R(\epsilon,\omega)\times\mathrm{Im}D^R(\mathbf{q},\omega)\mathrm{Im}G^A(\mathbf{p},\epsilon)\mathrm{Im}G^A(\mathbf{p}+\mathbf{k},\epsilon+\omega), \tag{31}$$

$$R(\epsilon,\omega)=N_\omega n_\epsilon(1-n_{\epsilon+\omega})-(1+N_\omega)(1-n_\epsilon)n_{\epsilon+\omega}. \tag{32}$$

Integrating, we present the result in a form

$$I_1(\epsilon)=\frac{3\pi^2\beta_t T^2}{(p_F u_t)(p_F l)}\frac{\tau}{\tilde{\tau}}\int d\omega_q R(\epsilon,\omega_q)\Phi_1, \tag{33}$$

where $\Phi_1(q)=1$, and the dimensionless coupling constant is given by

$$\beta_t=\beta_l\left(\frac{u_l}{u_t}\right)^2=\left(\frac{2\epsilon_F}{3}\right)^2\frac{\nu}{2\rho u_t^2}, \tag{34}$$

where $u_{t(l)}$ is the transverse (longitudinal) sound velocity.

The contribution of the second diagram may be also presented in a form of Eq. (33), where Φ_1 is changed by

$$\Phi_2=-\frac{3}{2}\frac{\tau}{\tilde{\tau}}[\zeta_0(q,\omega_q)-\zeta_2(q,\omega_q)]. \tag{35}$$

For Debye phonon spectrum $\omega_q<<qv_F$, and $\zeta_0(q,\omega_q)=\zeta_0(ql)=\arctan(ql)/(ql)$. Therefore, Φ_2 depends only on the one dimensionless parameter $x=ql$,

$$\Phi_t(x)=\Phi_1+\Phi_2=1+\frac{\tau}{\tilde{\tau}}\frac{3x-3(x^2+1)\arctan(x)}{2x^3}. \tag{36}$$

The inelastic electron relaxation rate is determined as

$$\frac{1}{\tau_{e\text{-}ph}(\epsilon)} = -\frac{\delta I(\epsilon)}{\delta n_\epsilon}(n_\epsilon = n_\epsilon^{eq}), \tag{37}$$

where n_ϵ^{eq} is the equilibrium distribution function. Using Eqs. (30), (33), and (36), we present the energy relaxation rate of electrons interacting with transverse phonons as

$$\frac{1}{\tau_{e\text{-}t.ph}(0)} = \frac{3\pi^2\beta_t T^2}{(p_F u_t)(p_F l)}\frac{\tau}{\tilde{\tau}}F_t(q_T l), \tag{38}$$

$$F_t(z) = \frac{4}{\pi^2}\int_0^{A_t} dx \Phi_t(xz)(N_x + n_x^{eq})x, \tag{39}$$

where $A_{t(l)} = \theta_D l/u_{t(l)}z$ (θ_D is the Debye temperature).

If $T << \theta_D$, the function $F_t(q_T l)$ is

$$F_t(q_T l) = \begin{cases} 1, & Tl > u_t \\ \left(1 - \dfrac{\tau}{\tilde{\tau}}\right) + \dfrac{\pi^2}{10}\dfrac{\tau}{\tilde{\tau}}(q_T l)^2, & Tl < u_t. \end{cases} \tag{40}$$

Now we consider the interaction of electrons and longitudinal phonons. In the pure material the interaction is described by the third diagram. In the general case this diagram is given by

$$I_3(\epsilon) = \frac{8}{\pi\nu}\int \frac{d\mathbf{p}d\mathbf{q}d\omega}{(2\pi)^7}\,\mathrm{Im}G^A(\mathbf{p},\epsilon)\mathrm{Im}\,G^A(\mathbf{p}+\mathbf{q},\epsilon + \omega)\mathrm{Im}D^R(\mathbf{q},\omega)(g)^2 R(\epsilon,\omega). \tag{41}$$

Integrating, we present the result as

$$I_3(\epsilon) = -\frac{\beta_l T^3}{(p_F u_l)^2}\int d\omega_q R(\epsilon,\omega_q)\Phi_3, \tag{42}$$

where $\Phi_3 = q l \zeta_0(q,\omega_q)$, and the dimensionless coupling constant is $\beta_l = \beta_t u_t^2/u_l^2$. Contributions of all other diagrams may be presented in the form of Eq. (42) with the following functions $\Phi_i(ql)$:

$$\Phi_1(y) = \frac{3}{y}\frac{\tau}{\tilde{\tau}},\quad \Phi_2(y) = -\frac{9\zeta_2^*}{y}\left(\frac{\tau}{\tilde{\tau}}\right)^2, \tag{43}$$

$$\Phi_4(y) = \Phi_6(y) = 3i\zeta_1^*\frac{\tau}{\tilde{\tau}}, \tag{44}$$

$$\Phi_5(y) = y\zeta_0^*\left(\frac{\zeta_0^*}{1-\zeta_0^*} - \frac{3}{y^2}\frac{\tau}{\tilde{\tau}}\right), \tag{45}$$

$$\Phi_7(y) = 3i\zeta_1^*\frac{\tau}{\tilde{\tau}}\left(\frac{\zeta_0^*}{1-\zeta_0^*} - \frac{3}{y^2}\frac{\tau}{\tilde{\tau}}\right). \tag{46}$$

Other diagrams give zero contribution.

Finally, the energy relaxation rate of electrons interacting with longitudinal phonons is

$$\frac{1}{\tau_{e\text{-}l.ph}(0)} = \frac{7\pi\zeta(3)}{2}\frac{\beta_l T^3}{(p_F u_l)^2}F_l(q_T l), \tag{47}$$

$$F_l(z) = \frac{2}{7\zeta(3)}\int_0^{A_l} dx \Phi_l(xz)(N_x + n_x)x^2, \tag{48}$$

$$\Phi_l(x) = \frac{2}{\pi}\left(\frac{x\arctan(x)}{x - \arctan(x)} - \frac{3}{x}\frac{\tau}{\tilde{\tau}}\right). \tag{49}$$

In the limiting cases the function $F_l(q_T l)$ is given by

$$F_l = \begin{cases} 1, & Tl > u_l \\ \dfrac{2\pi^3}{35\zeta(3)}(q_T l) + \dfrac{3\pi}{7\zeta(3)}\left(1 - \dfrac{\tau}{\tilde{\tau}}\right)(q_t l)^{-1}, & Tl < u_l. \end{cases} \tag{50}$$

According to Eqs. (38) and (47) in the impure case ($Tl < u_l, u_t$), the electron-phonon scattering rate is

$$\frac{1}{\tau_{e-ph}(0)} = \frac{\pi^4 T^4}{5}(p_F l)\left(\frac{\beta_l}{(p_F u_l)^3} + \frac{3\beta_t}{2(p_F u_t)^3}\frac{\tau}{\tilde{\tau}}\right) + \frac{3\pi^2 T^2}{2p_F l}\left(1 - \frac{\tau}{\tilde{\tau}}\right)\left(\frac{\beta_l}{p_F u_l} + \frac{2\beta_t}{p_F u_t}\frac{\tau}{\tilde{\tau}}\right). \tag{51}$$

IV. DISCUSSION

We have calculated the electron energy relaxation rate in a disordered conductor with the static and vibrating random-scattering potentials. Our main results are presented by Eqs. (38) and (47). The relative part of the vibrating potential with respect to the total potential is given by the parameter $k = \tau/\tilde{\tau}$. If the whole potential is dragged by phonons ($k = 1$), we reproduce the Pippard's equations for sound attenuation [Eqs. (36) and (50)], and the Schmid results for the electron relaxation rate. If $k < 1 - (Tl/u)^2$, the relaxation rate drastically changes at low temperatures. According to Eq. (51), it follows the T^2/l law.

If the scattering potential is static ($k = 0$), then only longitudinal phonons interact with electrons, and again at low temperatures $1/\tau_{e-ph} \propto T^2/l$. However, our results are different from the impurity renormalization of the pure electron-phonon vertex.[13] In particular, predicted in Ref. 13, modification of the energy relaxation rate to T^4 law at ultralow temperatures $T \sim u_l^2/v_F^2\tau$ (where $\omega_q \sim Dq^2$) is absent in our model. Taking into account screening of bare electron-phonon vertex, we found that the diffusion factor $i\omega + Dq^2$ in the renomalized vertex is canceled by the same factor in the dielectric function.

It is important to note that transverse phonons dominate in the relaxation over a wide temperature range, if $k > (u_t/u_l)^3/2 \sim 0.05$. In the case of incomplete drag of scatterers, the relaxation rate shows T^2/l law in both asymptotics,

$$\frac{1}{\tau_{e\text{-}t.ph}(0)} = \frac{3\pi^2\beta_t T^2}{(p_F u_t)(p_F l)} \times \begin{cases} k, & T \gg u_t/l \\ k(1-k), & T \ll u_t/l. \end{cases} \tag{52}$$

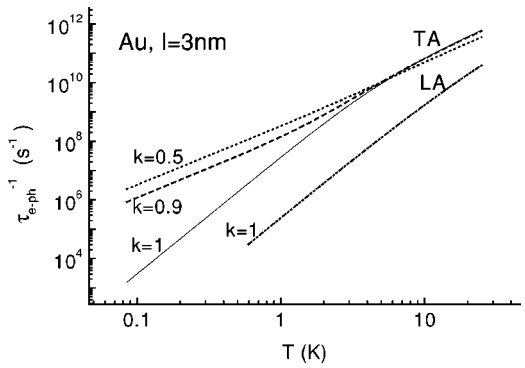

FIG. 6. Temperature dependence of the electron-phonon energy relaxation rate in Au films with the electron mean free path $l=3$ nm and different values of the parameter $k=\tau/\tilde{\tau}$: $k=1$ (complete drag of the scattering potential), solid curve; $k=0.9$, dashed curve; and $k=0.5$, dotted curve. Dashed-dotted curve is the contribution of longitudinal phonons ($k=1$).

At the intermediate temperatures, $T\sim u_t/l$, the exponent in the temperature dependence is larger than 2.

To illustrate our results, we calculate the electron-phonon relaxation rate in Au films. We use the following parameters of Au, taken from Ref. 6: $u_l=3.2\times10^5$ cm/s, $u_t=1.2\times10^5$ cm/s, $v_F=14\times10^7$ cm/s, $\beta_l=0.2$, and $\beta_t=1.4$. Temperature dependence of the electron-phonon relaxation rate in the Au film with the electron mean free path $l=3$ nm is presented in Fig. 6. As it was stressed in Ref. 6, in conductors with a small value of the electron mean-free path the electron interaction with transverse phonons due to vibrating impurities significantly dominates over the interaction with longitudinal phonons. This relation between contributions of transverse and longitudinal phonons may be altered only at very small values of $k(k<0.05)$, which will not be considered here. On Fig. 6 we present the relaxation rate for $k=0.5$,0.9, and 1. If the scattering potential is completely dragged by phonons ($k=1$), the relaxation rate is proportional to T^4 at $T\leqslant3$ K, and to T^2 at $T\geqslant20$ K. Low-temperature behavior is changed drastically in the case of incomplete drag. Even though $k=0.9$, the T^2 dependence is clearly seen at $T\leqslant2$ K. At the intermediate temperatures the function goes from one T^2 asymptote to another.

Figure 7 shows the dependence of the electron-phonon

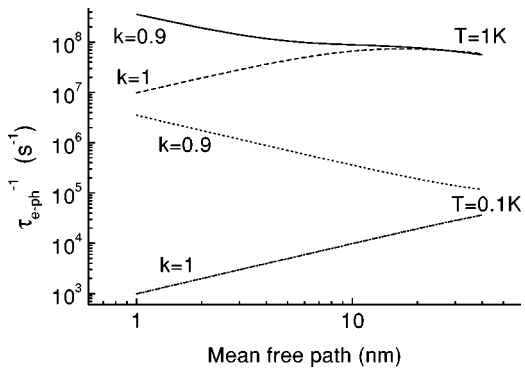

FIG. 7. Dependence of the electron-phonon relaxation rate on the electron mean free path (l) in Au films: solid curve, $T=1$ K,$k=0.9$; dashed curve, $T=1$ K,$k=1$; dotted curve, $T=0.1$ K,$k=0.9$; and dashed-dotted curve, $T=0.1$ K,$k=1$.

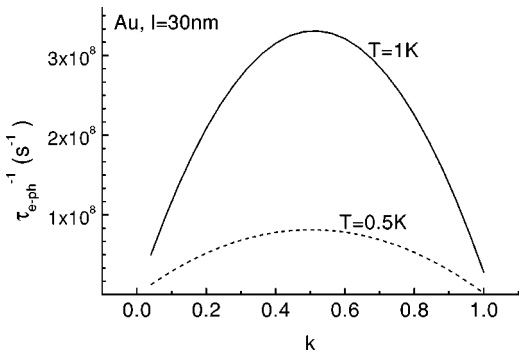

FIG. 8. Dependence of the electron-phonon relaxation rate on the parameter k: solid curve, $T=1$ K; dashed curve, $T=0.5$ K.

relaxation rate on the electron mean free path. As we discussed, if $k=1$, the interaction with transverse phonons results in the relaxation rate, which is proportional to T^4l at low temperatures and to T^2/l in the pure limit $T>u_t/l$. Therefore, at $k=1$ the l dependence is nonmonotonic with a maximum at $l\sim u_t/T$. As seen, at $T=1$ K, this maximum corresponds to $l\simeq20$ nm. In the case of incomplete drag of scatterers by phonons, the relaxation rate decreases in pure samples. Note, that the T^4 temperature dependence at $k=1$ is accompanied by l^1 dependence, while T^2 dependence at $k=0.9$ is attended by l^{-1} dependence.

The dependence of the relaxation rate on the parameter k at $T=0.5$ and 1 K is shown in Fig. 8. According to Eq. (52), if k is not very close to 0 or 1, it is given by the function $f(k)=k(1-k)$ with a prefactor, which is proportional to T^2/l. At very small k, the relaxation rate is determined by the contribution of longitudinal phonons. At k close to 1, according to Eq. (51) the relaxation rate is given by the T^4 term. Thus, the relaxation rate drastically drops in the regions $k<(u_t/u_l)^3$ and $k>1-(q_Tl)^2$.

Now we discuss experimental data. The T^2 temperature dependence of the electron-phonon scattering rate has been observed experimentally in various materials with a small value of the electron mean-free path: Au,[15–18] Ag and Mg,[18] Nb,[19] W,[8] CuCr,[20] $Ti_{1-x}Sn_x$, $Ti_{1-x}Ge_x$, $Ti_{0.97-x}Sn_{0.03}Sc_x$,[10,11,21,22] and $Sn_{1-x}Cu_x$.[23] In relatively pure materials ($l>10$ nm), at temperatures $T\geqslant10$ K this temperature dependence may be attributed to the interaction with transverse phonons in the clean limit of the Schmid theory ($q_Tl\geqslant1$). However, in Refs. 10, 11, and 17 the T^2 dependence has been found in the deep impure limit ($q_Tl<<1$). In our model these data correspond to the incomplete drag of impurities and defects in the investigated materials. The T^4 temperature dependence is rarely observed in experiments.[24,25] As we have seen, such dependence requires values of the parameter k to be very close to 1. Observed at low temperatures T^3 dependencies[26–28] are likely an indication of the transition region ($q_Tl\sim1$) for transverse phonons (see Fig. 6) rather than of the clean limit for longitudinal phonons.

Interpretation of effects of disorder on the relaxation rate is more complicated. Additional impurities and defects may change not only the electron mean free path, but also the parameter k. However, in any case the enhancement of the electron-phonon interaction in disordered samples evidences in favor of incomplete drag of the scattering potential by

phonons. Increase of the relaxation rate due to disorder has been observed in metallic films[10] and semiconducting low-dimensional structures.[9] In particular, the T^2/l dependence has been observed in TiAl and TiSn films.[10,22] Some experimental data[10] show that the relaxation rate is very sensitive to the microscopic quality of a particular sample: it depends not only on the electron mean free path, but also on the character of impurities and defects. In our model, the extent to which the scatterers are dragged by phonons is given by the parameter $k=\tau/\tilde{\tau}$, which may be used as a fitting parameter to describe experimental results over a wide temperature range. Experiments with pure metallic nanostructures at low temperatures would be also useful to study modification of the electron-phonon interaction due to electron-boundary scattering.

The strong dependence of the electron-phonon interaction on the impurity and defect concentration as well as on the character of scatterers opens possibilities to control the electron relaxation rate. At low temperatures, we expect a decrease in the relaxation rate due to substitutional disorder, and an increase due to heavy scatterers, such as columnar defects. Disorder-controlled electron-phonon relaxation is very perspective for many applications of thin-film electronics, such as hot-electron detectors and switches.[29,30]

ACKNOWLEDGMENTS

We acknowledge helpful discussions with M. Reizer and B. Karasik. The research was supported by the US ARO.

[1] A. Schmid, Z. Phys. **259**, 421 (1973).
[2] M.Yu. Reizer and A.V. Sergeev, Zh. Eksp. Teor. Fiz. **90**, 1056 (1986) [Sov. Phys. JETP **63**, 616 (1986)].
[3] J. Rammer and A. Schmid, Phys. Rev. B **34**, 1352 (1986).
[4] D. Belitz, Phys. Rev. B **36**, 2513 (1987).
[5] G. Grünvald and K. Scharnberg, Z. Phys. **268**, 197 (1974).
[6] N.G. Ptitsina, G.M. Chulkova, K.S. I'in, A.V. Sergeev, F.S. Pochinkov, E.M. Gershenzon, and M.E. Gershenson, Phys. Rev. B **56**, 10 089 (1997).
[7] K.S. Il'in, N.G. Ptitsina, A.V. Sergeev, G.N. Gol'tsman, E.M. Gershenzon, B.S. Karasik, E.V. Pechen, and S.I. Krasnosvobodtsev, Phys. Rev. B **57**, 15 623 (1998).
[8] A. Stolovits, A. Sherman, T. Avarmaa, O. Meier, and M. Sisti, Phys. Rev. B **58**, 11 111 (1998).
[9] A. Mittal, R.G. Wheeler, M.W. Keller, D.E. Prober, and R.N. Sacks, Surf. Sci. **361-362**, 537 (1996).
[10] C.Y. Wu, W.B. Jian, and J.J. Lin, Phys. Rev. B **57**, 11 232 (1998).
[11] S.Y. Hsu, P.J. Sheng, and J.J. Lin, Phys. Rev. B **60**, 3940 (1999).
[12] D. Belitz and M.N. Wybourne, Phys. Rev. B **51**, 689 (1995).
[13] B.L. Altshuler, Zh. Éksp. Teor. Fiz. **75**, 1330 (1978) [Sov. Phys. JETP **48**, 670 (1978)].
[14] Details of the Keldysh technique may be found in the following books: J. Rammer, *Quantum Transport Theory* (Perseus Books, Cambridge, MA, 1998); A.M. Zagoskin *Quantum Theory of Many-Body Systems* (Springer, New York, 1998).
[15] G. Bergmann, Solid State Commun. **46**, 347 (1983).
[16] J.P. Maneval, J. Desailly, and B. Pannetier, *Phonon Scattering in Condenced Matter* (Springer Verlag, Berlin, 1984), p. 43.
[17] B.I. Belevtsev, Yu.F. Komnik, and E.Yu. Beliayev, Phys. Rev. B **58**, 8079 (1998).
[18] R.P. Peters and G. Bergmann, J. Phys. Soc. Jpn. **54**, 3478 (1985).
[19] E.M. Gershenzon, M.E. Gershenzon, G.N. Goltsman, A.M. Lulkin, A.D. Semenov, and A.V. Sergeev, Zh. Éksp. Teor. Fiz. **97**, 901 (1990) [Sov. Phys. JETP **70**, 505 (1990)].
[20] J.F. DiTusa, K. Lin, M. Park, M.S. Isaacson, and J.M. Parpia, Phys. Rev. Lett. **68**, 1156 (1992).
[21] C.Y. Wu and J.J. Lin, Phys. Rev. B **50**, 385 (1994).
[22] J.J. Lin and C.Y. Wu, Europhys. Lett. **29**, 141 (1995).
[23] P.W. Watson and D.G. Naugle, Phys. Rev. B **51**, 685 (1995).
[24] R.A. Lee and M.N. Wybourne, J. Phys. F **16**, L169 (1986).
[25] Yu. F. Komnik, V.Yu. Kashirin, B.I. Belevtsev, and E.Yu. Beliaev, Phys. Rev. B **50**, 15 298 (1994).
[26] P. Santhanam and D.E. Prober, Phys. Rev. B **29**, 3733 (1984).
[27] M.L. Roukes, M.R. Freeman, R.S. Germain, R.C. Richardson, and M.B. Ketchen, Phys. Rev. Lett. **55**, 422 (1985).
[28] P.M. Echternach, M.R. Thoman, C.M. Gould, and H.M. Bozler, Phys. Rev. B **46**, 10 339 (1992).
[29] A.V. Sergeev and M.Yu. Reizer, Int. J. Mod. Phys. B **10**, 635 (1996).
[30] B.S. Karasik, W.R. McGrath, H.G. LeDuc, and M.E. Gershenson, Supercond. Sci. Technol. **19**, 745 (1999).